Reaction Chemistry & Engineering

Metal Cations as Inorganic Structure-Directing Agents during the Synthesis of Phillipsite and Tobermorite

Journal:	*Reaction Chemistry & Engineering*
Manuscript ID	RE-ART-10-2022-000466.R1
Article Type:	Paper
Date Submitted by the Author:	09-Feb-2023

Complete List of Authors:	Vega-Vila, Juan Carlos; University of California at Los Angeles, Department of Chemical and Biomolecular Engineering Holkar, Advait; University of California at Los Angeles, Department of Chemical and Biomolecular Engineering Arnold, Ross; University of California, Los Angeles, Department of Civil and Environmental Engineering Prentice, Dale; University of California Los Angeles, Civil and Environmental Engineering Dong, Shiqi; University of California Los Angeles Tang, Longwen; University of California Los Angeles La Plante, Erika; The University of Texas at Arlington, Materials Science and Engineering Ellison, Kirk; Electric Power Research Institute Inc Charlotte Kumar, Aditya; Missouri University of Science and Technology, Materials Science and Engineering Bauchy, M.; University of California Los Angeles, Srivastava, Samanvaya; UCLA, Chemical and Biomolecular Engineering Sant, Gaurav; University of California, Los Angeles, Department of Civil and Environmental Engineering Simonetti, Dante; University of California at Los Angeles, Department of Chemical and Biomolecular Engineering

Metal Cations as Inorganic Structure-Directing Agents during the Synthesis of Phillipsite and Tobermorite

Juan Carlos Vega-Vila[1,2], Advait Holkar[2], Ross A. Arnold[1,2,3], Dale Prentice[1,3], Shiqi Dong[1,3], Longwen Tang[3], Erika Callagon La Plante[4], Kirk Ellison[5], Aditya Kumar[6], Mathieu Bauchy[3], Samanvaya Srivastava[1,2,8]*, Gaurav Sant[1,3,7,8], Dante Simonetti[1,2]*

[1] Institute for Carbon Management (ICM), University of California, Los Angeles, CA, USA
[2] Department of Chemical and Biomolecular Engineering, University of California, Los Angeles, CA, USA
[3] Department of Civil and Environmental Engineering, University of California, Los Angeles, CA, USA
[4] Department of Materials Science and Engineering, University of Texas at Arlington, TX, USA
[5] Electric Power Research Institute (EPRI), Charlotte, NC, USA
[6] Department of Materials Science and Engineering, Missouri University of Science and Technology, Rolla, MO, USA
[7] Department of Materials Science and Engineering, University of California, Los Angeles, CA, USA
[8] California Nanosystems Institute (CNSI), University of California, Los Angeles, CA, USA

* Corresponding author. E-mail: dasimonetti@ucla.edu; samsri@ucla.edu

Abstract

Synthesis of structured porous materials in the absence of organic structure-directing agents highlights the adaptable nature of metal cations during hydrothermal synthesis. Here, we perform template-free hydrothermal treatments to synthesize phillipsite and tobermorite, at the same molar precursor ratios, while varying the identity and compositions of the counterbalancing metal cations that act as inorganic structure-directing-agents. Phillipsite is crystallized selectively at low total cationic charges (in the recovered solids) in the presence of sodium and potassium at 373 and 393 K. Partial substitution of sodium and potassium with calcium in the synthesis gels results in the co-precipitation of tobermorite phases in proportion to the calcium substitution amount; exclusive tobermorite precipitation was observed from synthesis growth solutions containing only calcium (373 and 393 K). X-ray diffraction (XRD) patterns, together with nitrogen adsorption isotherms (at 77 K), indicate a monotonic increase in the fraction of tobermorite crystals with increasing calcium content in synthesis gels. Differences in framework topology, dictated by the choice of metal cation, are accentuated by the quantity of metal cation retention within the available and interfacial cavities of phillipsite ((K + Na + Ca)/Al ≤ 1) and tobermorite (((K + Na + Ca)/Al ≥ 1). These results demonstrate the ubiquitous roles of metal cations during crystallization processes and their use to judiciously synthesize porous materials of varied framework topology.

1. Introduction

Structurally defined materials impart varying stages of complexity and functionality to inorganic solids. The addition of porous structures, as in the case of zeolitic materials, provide the capabilities to perform adsorption processes[1] and contribute favorable reaction cavities for catalytic chemical transformations.[2] It is therefore of general interest to control the structure and size of the porous cavities, largely targeted by judicious choices of synthesis conditions and parameters.

Synthesis of zeolitic materials is generally performed in basic media in the presence of metal precursors and an organic structure-directing agent (OSDA).[3] Silicon and metal precursors dissociate to form amorphous particles[4] that organize around structure-directing agents (SDA) during aging stages[5,6] prior to crystallization of the desired zeolite topology at elevated temperatures ($\geq$ 373 K).[7] The crystallization mechanism by which SDA-free synthesis takes place, however, is a result of complex phenomena. Metal cations (e.g., Na^+, K^+, Ca^{2+}) are typically used as a source of counterbalancing charge for the incorporation of Al heteroatoms into the framework during crystallization processes;[8] yet, they also occupy local cavities and serve as SDAs.[9] The nature of these molecular interactions and the proportionality between the fraction of metal cations used as SDA and for Al counterbalancing requires further investigation.

Phillipsite and tobermorite exemplify the key aspects of synthesis protocols that lead to crystallization of porous, inorganic materials in the absence of an OSDA. Phillipsite precipitates in the presence of sodium,[10] potassium,[10,11] and/or calcium;[12] yet, naturally-occurring phillipsite contains predominantly only sodium and potassium.[10] Tobermorite, in contrast, is a porous solid that is synthesized at similar synthesis gel molar compositions (e.g., 0.38 Na_2O: 0.19 K_2O: 0.05 Al_2O_3: 1 SiO_2: 17.57 H_2O for phillipsite[13] and 0.83 Ca: 1 Si: 18.2 H_2O for tobermorite[14,15]) and

temperatures (e.g., 373-393 K) but in growth solutions containing only calcium. Though the syntheses of these porous solids have similar inorganic content (in the synthesis gel), the synthesis conditions that dictate the crystallization selectivity towards phillipsite or tobermorite provide an opportunity to investigate the characteristics of inorganic SDAs to drive crystallization of porous structures.

Here, we develop synthesis protocols to discern the structural connections between phillipsite and tobermorite. We prepared zeolitic samples with varying cationic content (i.e., $(2 \times Ca^{2+})/(K^+ + Na^+ + (2 \times Ca^{2+}))$) in the absence of an organic SDA. Our results indicate that in the absence of calcium, phillipsite is the predominant phase crystallized at 373 and 393 K, whereas tobermorite is the predominant phase crystallized in the absence of sodium and potassium. A monotonic increase in the calcium content reflects a systematic increase in the fraction of tobermorite in the recovered solids, and concomitant increase in the total cationic content occluded in the crystalline solids. Our results indicate that potassium has a predominant role as an Al counterbalance cation, while sodium and calcium have a predominant role as SDA. Taken together, these results highlight the versatility of metal cations as charge balancing agents and inorganic SDAs during zeolite crystallization processes.

2. Experimental Methods

2.1. Catalyst synthesis

Phillipsite zeolites (PHI-TOB-373/393-0) were synthesized by adapting the procedure reported by Cichocki et al.[13] In a typical synthesis, potassium hydroxide (KOH, Fisher Scientific, ≥ 85%) was added to deionized water (18.2 MΩ) and stirred until completely dissolved in a

Nalgene™ wide-mouth HDPE bottle (250 cm^3, Thermo Fisher Scientific). Then, sodium aluminate (Sigma Aldrich, 50-56% Al_2O_3, 40-45% Na_2O) was added and the resulting mixture was stirred until completely dissolved. Lastly, sodium silicate (Sigma Aldrich, 26.5% SiO_2, 10.6% Na_2O) was added to the Nalgene container. The resulting gel solution was covered and stirred for 24 h at ambient conditions. The final gel composition was 6.95 Na_2O: 3.5 K_2O: 1 Al_2O_3: 18.5 SiO_2: 325 H_2O. The gel was placed into a Teflon-lined stainless-steel autoclave and heated to 373 or 393 K for 7 days under static conditions. The recovered solids were washed thoroughly with water, isolated by centrifugation, and dried overnight at 363 K.

The charge ratio (C.R. = $(2 \times Ca^{2+})/(K^+ + Na^+ + (2 \times Ca^{2+}))$, or the amount of calcium in the synthesis gel, was modified by adapting synthesis procedures reported for phillipsite synthesis by Cichocki et al.[13] In a typical synthesis, KOH was added to deionized water and stirred until completely dissolved in a Nalgene bottle (250 cm^3). Then, sodium hydroxide (NaOH, Fisher Scientific, ≥ 97%) was added and the resulting mixture was stirred until completely dissolved. Calcium hydroxide ($Ca(OH)_2$, Fisher Scientific, ≥ 98.5%) and aluminum hydroxide ($Al(OH)_3$, Strem Chemicals, 87.8%) were added individually and the mixture was stirred until complete dissolution. Lastly, Ludox SM30 (Sigma Aldrich, 30 wt.% in water) was added to the Nalgene container. The resulting gel solution was covered and stirred for 24 h at ambient conditions. The final gel composition was x Na_2O: y K_2O: z CaO: 1 Al_2O_3: 18.5 SiO_2: 325 H_2O, where x, y, and z were modified to attain the desired charge ratios (e.g., 0.25-0.80). The alkaline content (e.g., OH/Si) in the starting synthesis gels was kept constant for samples crystallized at the same temperature (details in Section S.1, Supporting Information). The specific gel compositions for all the samples in this study are compiled in Table S.1 (Supporting Information). The gel was placed into a Teflon-lined stainless-steel autoclave and heated to 373 or 393 K for 7 days under static

conditions. The recovered solids were washed thoroughly with water, isolated by centrifugation, and dried overnight at 363 K.

Tobermorite silicate hydrates (PHI-TOB-373/393-1) were synthesized by adapting the procedure reported previously.[14–19] In a typical synthesis, $Ca(OH)_2$ was added to deionized water and stirred until completely dissolved in a Nalgene bottle. Then, Ludox SM30 was added and the resulting mixture was stirred until completely dissolved. At 373 K (PHI-TOB-373-1), $Al(OH)_3$ was added and the resulting solution was stirred until complete dissolution (0.11 Al_2O_3: 0.90 CaO: 1 SiO_2: 17.59 H_2O). The resulting gel solution was covered and stirred for 24 h at ambient conditions. The final gel composition of synthesis gels prepared in the absence of aluminum at 393 K was 0.83 CaO: 1 SiO_2: 18.2 H_2O. The gel was placed into a Teflon-lined stainless steel autoclave and heated to 373 or 393 K for 7 days under static conditions. The recovered solids were washed thoroughly with water, isolated by centrifugation, and dried overnight at 363 K.

For simplicity, samples are referred to as PHI-TOB-X-Y, where X represents the temperature at which the hydrothermal treatment was performed (e.g., 373 K or 393 K) and Y represents the charge ratio (fraction of calcium in the total cationic content).

2.2. Zeolite Characterization

Powder X-ray diffraction (XRD) patterns were collected in the range 5-70° of 2θ (scan rate of 0.0765° s^{-1} and a step size of 0.02°) using a PANalytical X'PertPro X-ray diffractometer with a Cu Kα x-ray source ($\boldsymbol{\alpha}$ = 1.54 Å) and an X'Celerator 2 detector.

Vapor-phase N_2 (77 K) adsorption isotherms were collected with a Micromeritics TriStar II 3020 instrument. Typically, ~0.20 g of zeolite sample, pelleted and sieved to retain particles with size between 180-250 μm, were degassed by heating under vacuum (<0.1 Torr) to 383 K for 24 h

prior to adsorption measurements. The micropore volume was determined from semi-log derivative analysis of the isotherm ($\partial(V_{ads}/g)/\partial(\log(P/P_0)$ vs. $\log(P/P_0)$), where the first maximum represents the micropore filling transition and the subsequent minimum represents the end of micropore filling.

The elemental composition of the recovered solids was measured using an inductively-coupled-plasma optical emission spectrometer (ICP-OES, Varian Vista-MPX). Samples (~0.03g) were dissolved overnight in 2 g of HF (48 wt.%, Alfa Aesar) and diluted with ~50 g of deionized water. In a separate 15 cm^3 centrifuge tube, ~10 g of the resulting solution and 0.1 g of nitric acid were mixed prior to measurements. The Si/Al ratios of PHI-TOB-373/393-0 were calculated using the unit cell formula for the PHI framework topology.

Transmission electron microscope (TEM) images were collected after samples (< 20 mg) were dispersed in ethanol for 240 s in an ultrasonic bath. Approximately 4 drops of the dispersion were deposited in a 200 mesh Cu grid with a C film. TEM bright field images were taken with a JEOL JEM-2100F TEM/STEM operated at 200 keV, with spot size 1 and magnifications between 12 and 20kx.

3. Results and Discussion

3.1. Roles of metal cations on the crystallization of phillipsite and tobermorite aluminosilicates

Samples are denoted as PHI-TOB-X-Y, where X represents the temperature of the hydrothermal treatment (e.g., 373 K or 393 K) and Y represents the charge ratio, defined as the fraction of calcium in the total cationic content of the synthesis gels ($(2 \times Ca^{2+})/(K^+ + Na^+ + (2 \times Ca^{2+})$), see experimental section). Hydrothermal treatments of synthesis gels associated with

phillipsite crystallization were performed at 373 and 393 K in the sole presence of sodium and potassium (PHI-TOB-373/393-0), and the structure of the recovered solids was probed using X-ray diffraction (XRD) patterns and nitrogen adsorption isotherms (77 K). Figure 1 encloses the XRD patterns of the recovered solids of all the samples prepared in this study. XRD patterns of PHI-TOB-373/393-0.0 show primary diffraction peaks centered at 28.1 and 30.5˚ (Figure 1(A)), previously observed for zeolitic samples with a phillipsite topology.[20] Micropore volumes (Figure 2), measured from the semi-log derivative plot of the nitrogen adsorption isotherm (77 K, Section S.2, Supporting Information), are also characteristic of phillipsite zeolites (0.003 $cm^3\ g^{-1}$).[21–23] Characteristic phillipsite prism-like and lath-like morphologies[24] were detected with transmission electron microscopy (TEM) images (Section S.3, Supporting Information). The precipitation of inorganic solids with structural features of phillipsite indicate that, in the absence of organic structure-directing agents (OSDA), it is the predominant zeolitic phase crystallized in the presence of sodium and potassium (373 K, 168 h) as the only cationic charges in growth solutions.

Phillipsite, as a natural and synthetic zeolite, crystallizes in the presence of sodium, potassium, and/or calcium.[10–12] To further probe the role of the metal cations in the crystallization processes that lead to phillipsite formation, hydrothermal treatments were performed by replacing the total cationic contributions of sodium and potassium in growth solutions with calcium. Performing hydrothermal syntheses at the same total cationic charge ($Na_2O + K_2O = 10.45$) but replacing the total metal cations with calcium ($CaO = 5.23$) resulted in XRD patterns (Figure 1) and micropore volumes (Figure 2) that are different from those observed in the sole presence of sodium and potassium (Figure 1). Specifically, XRD patterns of PHI-TOB-373/393-1.0 have distinctive diffraction peaks centered at 29.4 and 49.9˚, and 10× higher micropore volumes (~0.07 $cm^3\ g^{-1}$, Section S.2, Supporting Information). TEM images of the recovered solids illustrate an

189 acicular morphology (Section S.3, Supporting Information). These XRD patterns, micropore
190 volumes, and morphological parameters are characteristic of Al-tobermorite (referred as
191 tobermorite in this manuscript) silicate hydrates.[14,15,25–27]

192 The topological characteristics of hydrothermally-synthesized zeolites are dictated by the
193 molar composition of synthesis precursors in the synthesis gel and the conditions of the
194 hydrothermal treatment.[5,28] The pH of the synthesis growth solution during crystallization
195 processes, in particular, influences the final Al content (i.e., Si/Al content) and the structural
196 properties of the resulting zeolitic material, and it can be modified during crystallization processes
197 by modifications in the alkaline content (e.g., OH/Si).[5,28,29] In this study, the alkaline content and
198 solution charge $((K^+ + Na^+ + (2 \times Ca^{2+}))/Al)$ in synthesis gels prior to high temperature treatments
199 were fixed for each synthesis series (e.g., crystallized at the same temperature) to mitigate
200 contributions provided by the thermodynamic crystallization of different zeolitic phases at varied
201 pH (Section S.1, Supporting Information). Phillipsite molecular sieves and tobermorite silicate
202 hydrates crystallize at similar pH ranges (13-14),[30,31] congruent with coprecipitation mechanisms
203 observed in this work. These synthetic strategies, at fixed alkaline content, provide frameworks to
204 investigate the influence of the identity of metal cations in the starting synthesis growth solutions
205 on the transition from phillipsite zeolites to tobermorite silicate hydrates after hydrothermal
206 treatments (at 373 and 393 K).

207 Metal cations in synthesis gels have varied roles during hydrothermal processes in the
208 absence of OSDAs. An illustration of the roles of metal cations in the microporous cavities of
209 phillipsite after heat treatments (373 K, 168 h) is enclosed in Scheme 1. Isomorphous substitution
210 of aluminum heteroatoms in siliceous frameworks results in a localized anionic charge on an
211 adjacent oxygen imparted by differences in the oxidation state of silicon (Si^{4+}) and aluminum

(Al^{3+}) when tetrahedrally-coordinated. The first role of metal cations is to compensate this mismatch in framework charges imparted by aluminum incorporation. This counterbalancing role takes place using monovalent cations (e.g., Na^+ and/or K^+) for aluminum that have no nearby aluminum neighbor ("isolated" aluminum, Al-O(-Si-O)$_x$-Al, $x \geq 3$) and divalent cations (e.g., Ca^{2+}) in frameworks that can accommodate aluminum heteroatoms separated by one or two silicon atoms ("paired" aluminum, Al-O(-Si-O)$_x$-Al, $x = 1, 2$).[32] In absence of OSDAs, as is the case in the syntheses performed in this study, metal cations organize within the microporous cavities during crystallization processes to become inorganic SDAs.

In synthesis gels of PHI-TOB-373/393-0.0, sodium and potassium account for aluminum counterbalance and as SDA, and we probed their total contribution through elemental analysis. Table 1 contains the elemental composition, collected via induced coupled plasma optical emission spectroscopy (ICP-OES), of the solids recovered for all the syntheses performed in this study. The potassium content is higher than the sodium content in samples prepared at varied temperatures (373 and 393 K), accounting for > 50% of the total cations retained with respect to the aluminum content. Although sodium is in excess (2:1 ratio) in synthesis gels when compared to potassium, the sodium content accounts for < 40% of the total cations in the solids relative to the retained aluminum.

The total cationic content, defined as the summation of all the metal cations normalized to the aluminum content, is ≤ 1 for samples prepared in the absence of calcium in growth solutions (PHI-TOB-373/393-0.0, Table 1). The implication of these results, collected after water washing steps intended to remove unreacted species, is that the remaining metal cations are participating as counterbalance cations for aluminum in the framework (assuming that all the aluminum is in a tetrahedral coordination) and those participating in a templating role have been selectively

235 removed during washing steps. Consequently, the elemental compositions of PHI-TOB-373/393-
236 0.0, together with the excess of sodium in growth solutions, suggest that the primary role of sodium
237 (Na/Al < 40%, Table 1) during hydrothermal treatments is as a SDA and gets removed during
238 washing steps. By extension, our results indicate that potassium (K/Al > 50%) has a predominant
239 role as an aluminum counterbalance cation during crystallization of phillipsite zeolites at 373 and
240 393 K. Zeolites prepared in the sole presence of calcium (PHI-TOB-373-1.0) also contain metal
241 cationic contents that account for less than the total aluminum content (Cat. / Al ≤ 1, Table 1),
242 suggesting that the retention of metal cations during tobermorite crystallization procedures are
243 predominantly associated with aluminum heteroatoms. Taken together, these results exemplify the
244 structure-directing role of metal cations in crystallization processes in the absence of SDAs.
245 Zeolite polymorphism driven by the judicious choice of inorganic SDAs highlights the
246 adaptable capabilities of metal cations in zeolite crystallization protocols.[28] Hydrothermal
247 treatments of growth solutions replacing sodium with potassium, for instance, leads to the
248 formation of NU-10 (TON) rather than MFI (523 K, 122 h),[33] synthesis gels containing potassium
249 instead of sodium crystallize EDI rather than LTA (468 K, 96 h),[34] and synthesis gels containing
250 varying mixtures of sodium and potassium crystallize LTA, SOD, and/or FAU (429 K, 168 h),[35]
251 amongst others.[28] Here, replacing sodium and potassium with calcium in synthesis gel
252 compositions that typically crystallize phillipsite,[13] results in the precipitation of tobermorite, a
253 silicate hydrate of different identity and pore structure. Although the elemental composition of
254 tobermorite prepared at 373 K (PHI-TOB-373-1.0) was expected to occlude more calcium content
255 (i.e., Ca/Al > 1) and at higher densities than those measured (Ca/Al < 1), the structure of the
256 characterized solid indicates the distinctive features (Figure 1) of tobermorite as a result of an
257 exclusive calcium-containing growth solution. Further experiments are required to interrogate the

differences between PHI-TOB-373-1.0 and other tobermorite samples crystallized in this study. Altogether, the results in this manuscript contribute guidelines for the preparation of two different zeolitic and silicate hydrate aluminosilicates by varying the metal cation identity in the synthesis gel. We next investigate the roles and contributions of inorganic SDAs by systematically modifying the metal cation content.

3.2. Guidelines for the selective co-precipitation of phillipsite and tobermorite

The total cationic content is defined as the molar composition in the synthesis gel composed by all metal cations. Systematic substitution of the cationic content with calcium, however, requires accounting for differences between monovalent cations (Na^+ and K^+) and divalent cations (Ca^{2+}). The role of calcium as a counterbalancing cation for aluminum incorporation is limited by the ability of a framework to accommodate two aluminum heteroatoms in close proximity (Al-O(-Si-O)$_x$-Al, x = 1, 2) in order for aluminum incorporation to take place. The calcium content in the synthesis gel was determined by half of the total molar contributions of sodium and potassium to retain the same total cationic charge in the synthesis gel; at the same time, the alkaline content within each synthesis series (e.g., crystallized at the same temperature), was kept constant for all samples prepared in this study (Section S.1, Supporting Information). We define the charge ratio in the synthesis gel as the fraction of the total cationic content composed by calcium (e.g., $(2 \times Ca^{2+})/(K^+ + Na^+ + (2 \times Ca^{2+}))$).

The transition from phillipsite to tobermorite phases was probed by performing hydrothermal syntheses at varied charge ratio in synthesis growth solutions. XRD patterns of samples prepared at varied charge ratio reflect diffraction peaks centered at 29.4° and 49.9° that increase concomitantly with increasing calcium content (Figure 1). Differences in framework

identity and composition are also detected in the pore volume measured by nitrogen adsorption isotherms, with a monotonic increase in the micropore volume from 0.003 to 0.03 $cm^3\ g^{-1}$ with increasing charge ratio (Figure 2). These results highlight single-step hydrothermal treatments to prepare silicate hydrates of mixed morphological and adsorption properties by tailoring the molar composition of metal cations in the starting synthesis growth solution (Section S.2, Supporting Information). The increase in XRD diffraction peaks associated with tobermorite (e.g., 29.4 and 49.9˚), together with micropore volumes that increase concomitantly, indicate that phillipsite crystallization transitions to tobermorite crystallization with increasing the calcium content in the synthesis gel, as we discuss next with respect to the elemental composition of the recovered solids.

Figure 3 compares the potassium and sodium content in the recovered solids, normalized by the aluminum content. Normalizing the cationic molar content by the aluminum content allows for rigorous distinctions of the relevance of sodium and potassium as aluminum counterbalance cations. The sodium content increases concomitantly with the potassium content in the recovered precipitates. The sodium and potassium content also increase monotonically with increasing charge ratio for samples crystallized at 393 K (PHI-TOB-393), as diffraction peaks (e.g., peaks centered at 29.4 and 49.9˚) associated with tobermorite increase concomitantly. These results indicate that the inclusion of sodium and potassium is codependent and that, although the combination of the two predominantly leads to crystallization processes associated with phillipsite, the retention of a higher fraction of these metal cations ((K + Na)/Al >1) is facilitated by tobermorite crystallization.

Figure 4 compiles the total cation content with respect to the sodium content (normalized to the aluminum content). The total cationic content increases systematically with respect to the sodium content (per aluminum), and thus with increasing the fraction of tobermorite precipitation.

Phillipsite phases are crystallized at total cationic charges (per Al) < 2, while tobermorite phases are primarily detectable at total cationic charges > 2. Retention of a higher content of metal cations at higher charge ratios, together with the formation of a higher fraction of tobermorite, suggests the bigger pores in tobermorite (~1 nm)[36] compared to phillipsite (8 MR, ~0.37 nm), or the mesoporous area between the two phases (observed in the hysteresis in N_2 adsorption isotherms in Section S.2, Supporting Information), encapsulate more metal cations during crystallization processes. These results suggest that phillipsite zeolites primarily retain inorganic cations associated with aluminum heteroatoms, while tobermorite silicate hydrates retain metal cations corresponding to aluminum counterbalance as well as those filling the available porous cavities (SDA role). These results indicate that, either because of structural composition or the ability to retain more cations within various topologies of varied pore structure, more cations are captured within the porous architecture of tobermorite silicate hydrates compared to phillipsite zeolites.

Differences in the identity and composition of metal cations in the starting synthesis growth solutions result in the precipitation of porous materials with varied structural and physicochemical properties. For samples of mixed phillipsite zeolites and tobermorite silicate hydrate phases, the micropore volume measurements and XRD patterns are similar to the weighted linear combination of the two phases (Figure 2), as previously observed for the intergrowth precipitation of SAPO-5/SAPO-11.[37] Compared to the physical mixture of the two phases, however, the hydrothermal treatments developed in this study impart capabilities to prepare mixed phases in a single step by tailoring the identity of the metal cations in the starting synthesis gel. The protocols described here, in addition, result in the crystallization of inorganic materials with available mesoporous cavities (Section S.2, Supporting information), because of the coprecipitation of both phases, enabling access to bigger voids that are beneficial to transport phenomena relevant for catalytic[38,39] and

adsorption[40,41] processes. The selective crystallization of both phases by replacing the cationic charge imparted by calcium in the starting synthesis gel suggests that crystallization mechanisms are sensitive to the identity of the metal cations in the starting growth solution, as we explore next.

Zeolite crystallization mechanisms and polymorphism are generally described by driving forces following the Ostwald rule of stages[42,43] or the transformation of crystalline phases guided by their molar density.[5,28,44] Crystallization following the Ostwald rule of stages take place after dissolution of synthesis precursors to form amorphous, metastable phases that reorganize over time in stages that form more thermodynamically stable phases (e.g., from structures of less negative to more negative enthalpy of formation).[42,43] In other instances, zeolite transformations occur by the formation of metastable phases that transform over time to form a phase with higher framework density (i.e., a framework with a lower molar volume).[44] In the phillipsite/tobermorite system studied here, we speculate that silicon and aluminum complexes, available in the synthesis gels after precursor dissolution during aging protocols (ambient, 24 h), nucleate metastable phases around inorganic cations. At the same time, the stabilized structure is dictated by the kinetic diameter, hydrated radii, or other physicochemical properties of the metal cations in solution (Scheme 2). These metastable phases, in turn, then dictate the aluminosilicate phase that eventually nucleates locally and crystallizes during high temperature treatments. We surmise that tobermorite, with bigger cavities than phillipsite, accommodates calcium cations and its crystallization results from high temperature treatments of aluminosilicate complexes formed around calcium during the aging step (Scheme 2). These proposed mechanistic steps, based primarily on the Ostwald rule of stages, describe general nucleation and crystallization steps that result in the crystallization of pure or mixed phillipsite and tobermorite phases in the presence of sodium, potassium, and/or calcium in varied composition in synthesis gels.

Distinguishing the ability of various metal cations to arrange within microporous and mesoporous voids allows for the preparation of porous aluminosilicates with varying pore structure. Sodium and potassium contribute to the selective crystallization of phillipsite zeolites in the absence of calcium (at 373 and 393 K). The total cationic content (normalized by Al) on PHI-TOB-373/393-0 samples suggest that the micropores of phillipsite accommodate cations exclusively to counterbalance aluminum heteroatoms. The higher total cationic content (per Al) on samples of varied charge ratio, together with detection of tobermorite phases, however, indicates that tobermorite phases retain metal cations associated with aluminum counterbalance and those that participate of structure-directing processes. The consistently higher total cationic content (per Al) in all the samples prepared at 393 K compared to those synthesized at 373 K, along with XRD features associated with tobermorite becoming prominent at low charge ratios (C.R. > 0.3), corroborate that tobermorite porous structures accommodate metal cations that participate in aluminum counterbalance and template roles. Taken together, this study summarizes guidelines for the preparation of zeolitic phases in the absence of OSDAs and highlights the ubiquitous roles of metal cations during crystallization processes of zeolitic materials.

4. Conclusions

Synthetic protocols involving zeolite crystallization take place around OSDAs that dictate the resulting topological properties of the precipitates. In the absence of OSDAs, however, inorganic SDAs can selectively nucleate and crystallize aluminosilicates of various framework topologies depending on their identity and synthesis conditions.[28]

Here, we elaborate on the roles of sodium, potassium, and calcium in the crystallization of phillipsite zeolites and/or tobermorite silicate hydrates (at 373 K and 393 K) at the same total molar cationic content. Phillipsite zeolites are selectively crystallized (at 373 K and 393 K) from starting growth solutions that contain solely sodium and potassium, and retain metal cations at molar ratios that account only for roles associated with of aluminum counterbalance during crystallization processes ($(Na + K)/Al \leq 1$). Tobermorite samples, however, are selectively crystallized after high temperature treatments (at 373 K and 393 K) of growth solutions containing solely calcium. Aluminosilicates containing tobermorite crystals retained metal cations at molar ratios ($(K + Na + Ca)/Al \geq 1$) indicating their ubiquitous roles as both aluminum counterbalance and SDA during crystallization protocols. Syntheses performed (373 K and 393 K) at mixed compositions of metal cations indicate that the partial substitution of sodium and potassium with calcium on synthesis gels (identical total molar compositions) results in the crystallization of mixed phillipsite and tobermorite phases. We surmise that these results are the consequence of the aluminosilicate complexes stabilized around metal cations during aging stages, leading to nucleation and crystallization of tobermorite when these complexes are encapsulating calcium cations and phillipsite when the complexes are isolating sodium and/or potassium. Taken together, these results summarize the roles of metal cations during crystallization processes and highlight the ability of their identity to dictate the topological properties, tailored for specific applications, of the resulting precipitate.

391 **Author contributions**

392 JCVV—Investigation, Writing – Original Draft; AH—Investigation; RA—Investigation, Writing
393 – Original Draft; DP—Writing – Review & Editing; SD—Investigation; LT—Investigation;
394 ELP—Conceptualization, Writing – Review & Editing, Funding acquisition; KE—Funding
395 acquisition; AK—Funding acquisition, Investigation; MB—Conceptualization, Funding
396 acquisition, Writing – Review & Editing; SS—Conceptualization, Writing – Original Draft and
397 Review & Editing, Funding acquisition, Supervision, Project administration; GS—
398 Conceptualization, Writing – Original Draft and Review & Editing, Funding acquisition,
399 Supervision, Project administration; DS—Conceptualization, Writing – Original Draft and
400 Review & Editing, Funding acquisition, Supervision, Project administration;
401
402
403 **Conflicts of interest**
404 There are no conflicts to declare
405
406
407 **Acknowledgements**
408 We acknowledge the financial support provided by the Advanced Research Projects
409 Agency-Energy (ARPA-E: Award Number: DE-AR0001147). We thank Dr. Joseph King and
410 Dr. Madhav Acharya for helpful technical discussions.
411

412 **Figures and Tables**

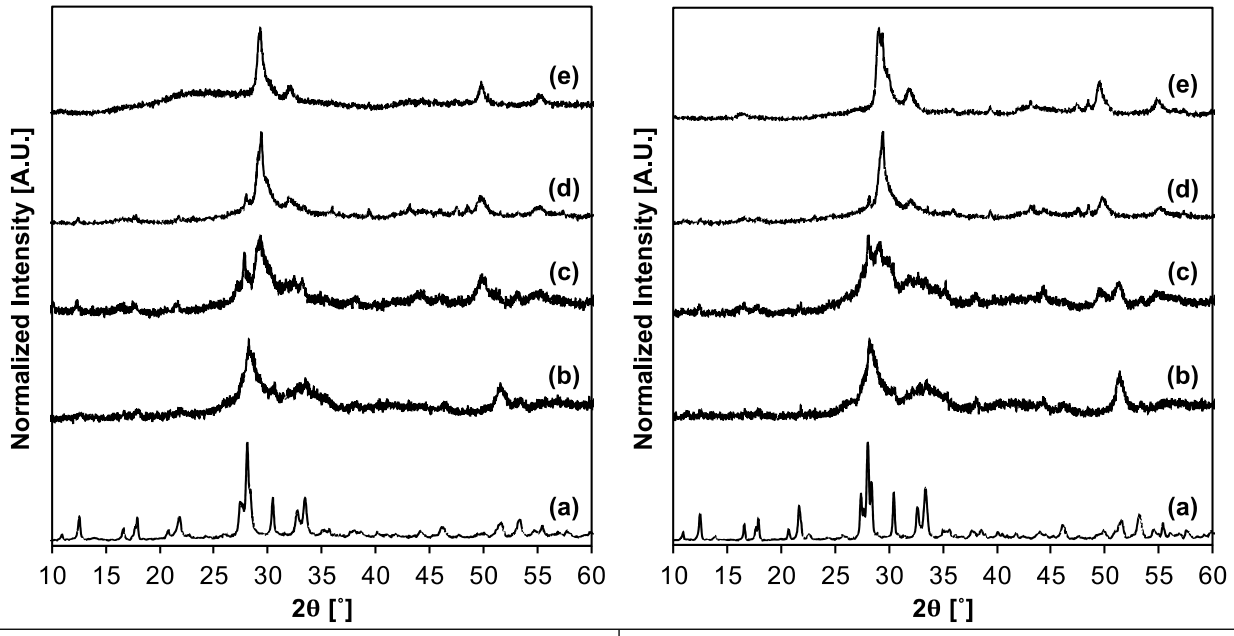

Figure 1. X-Ray Diffraction (XRD) patterns of (a) PHI-TOB-373-0, (b) PHI-TOB-373-0.25, (c) PHI-TOB-373-0.50, (d) PHI-TOB-373-0.75, and (e) PHI-TOB-373-1 crystallized at (A) 373 K, and of (a) PHI-TOB-393-0, (b) PHI-TOB-393-0.30, (c) PHI-TOB-393-0.50, (d) PHI-TOB-393-0.80, and (e) PHI-TOB-393-1 crystallized at (B) 393 K.

413
414

415

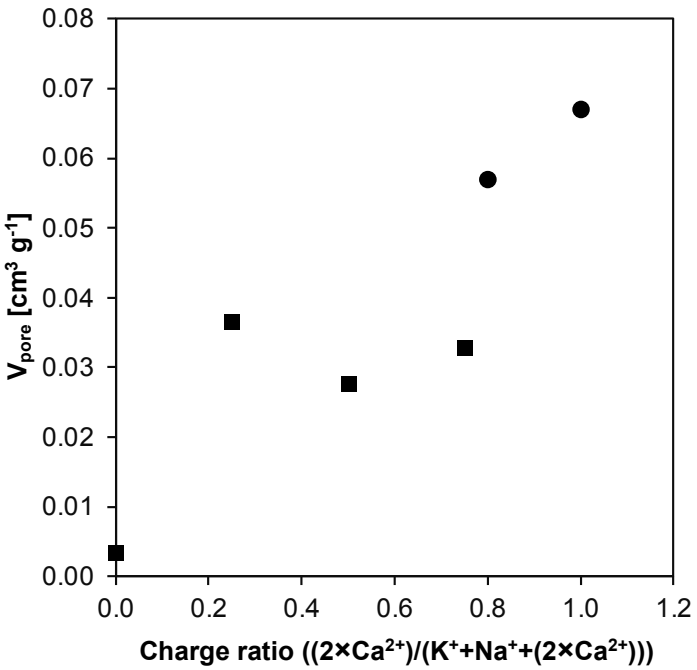

Figure 2. Micropore volume (cm^3 g^{-1}) of PHI-TOB-373 (□) and PHI-TOB-393 (●) with respect to the charge ratio (C.R. = (2 × Ca^{2+})/(K^+ + Na^+ + (2 × Ca^{2+})) in the starting synthesis growth solution.

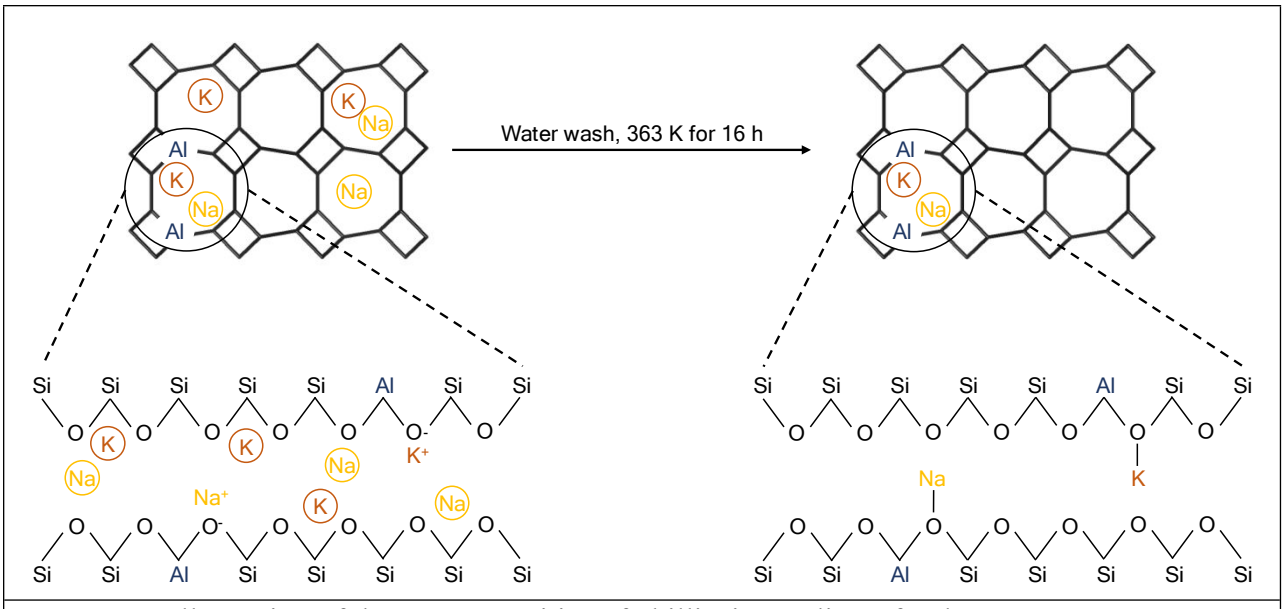

Scheme 1. Illustration of the porous cavities of phillipsite zeolites after heat treatments at 373 or 393 K (168 h) prior to and after water washing steps and drying procedures (363 K, 16 h).

418

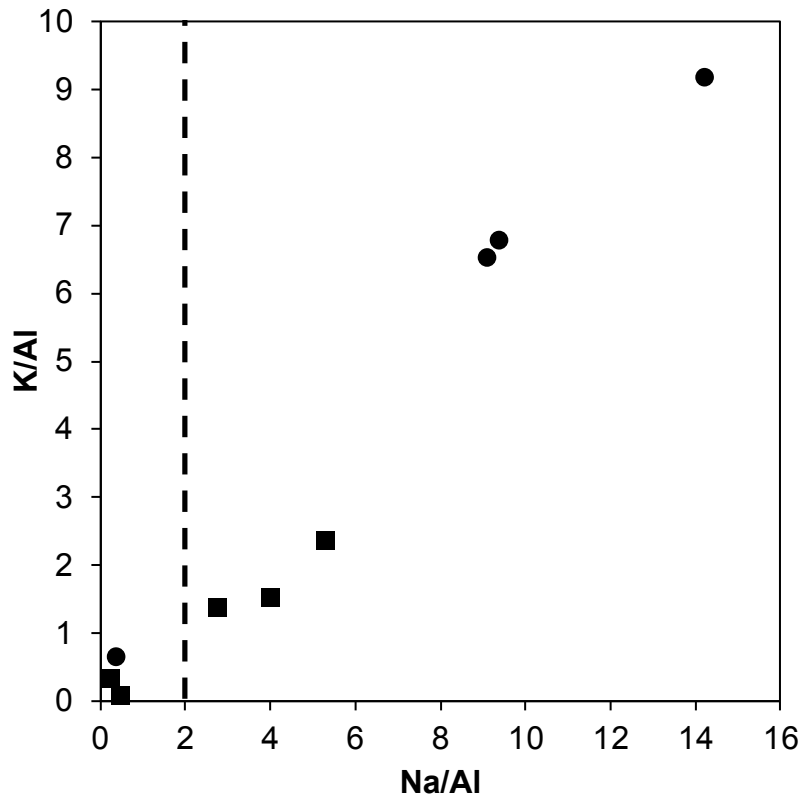

Figure 3. Potassium and sodium content normalized by the aluminum content in the recovered solids with varying the total charge ratio in hydrothermal treatments at 373 K (□) and 393 K (●). Shaded areas represent elemental compositions at which selective formation of one phase (e.g., phillipsite or tobermorite) is observed.

419

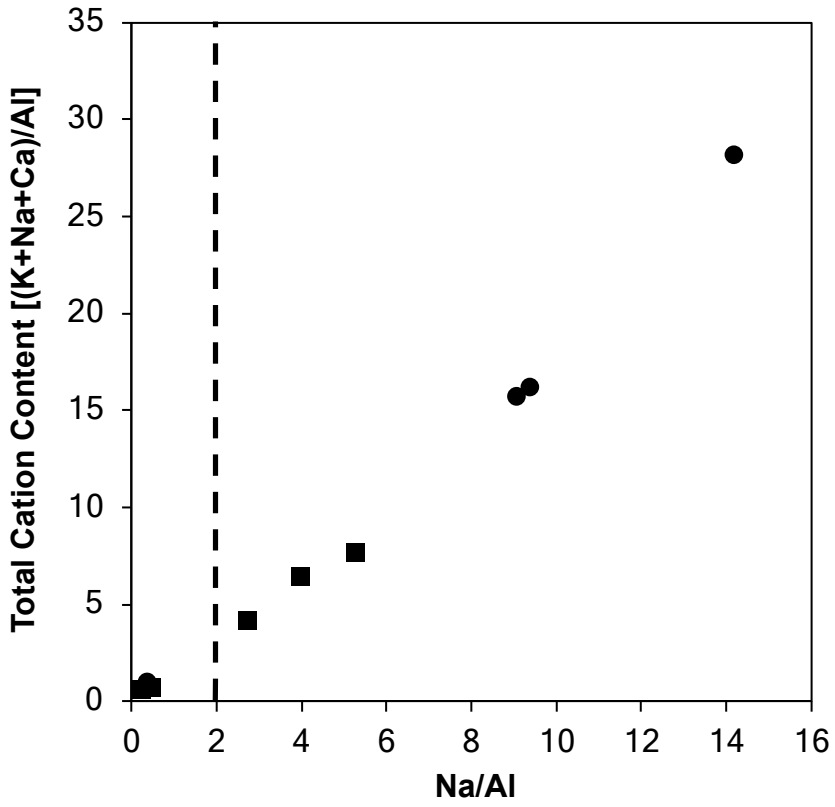

Figure 4. Total cation content and sodium content normalized by the aluminum content in the recovered solids with varying the total charge ratio after hydrothermal treatments at 373 K (□) and 393 K (●). The total cation content is defined as the summation of individual metal cations (e.g., sodium, potassium, and calcium) normalized by the aluminum content. Shaded areas represent elemental compositions at which selective formation of one phase (e.g., phillipsite or tobermorite) is observed.

420

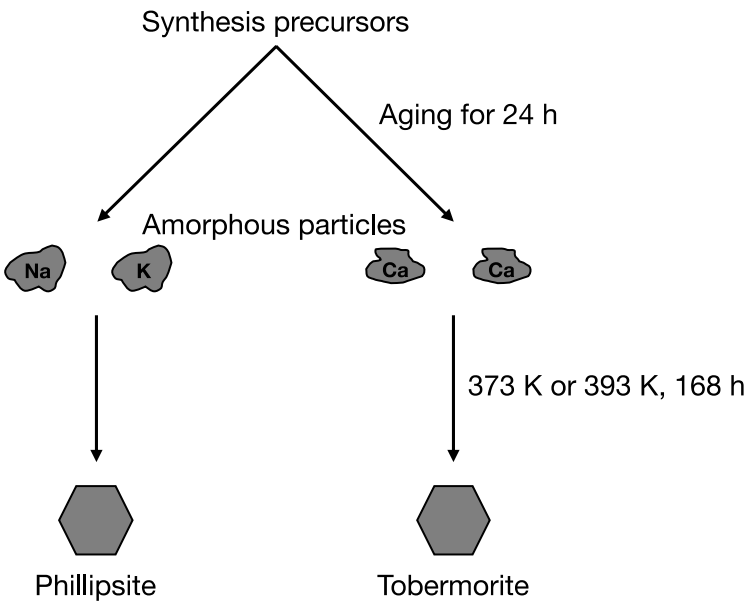

Scheme 2. Proposed mechanism for the crystallization of phillipsite and/or tobermorite (373 and 393 K, 168 h) in the presence of sodium, potassium, and calcium.

421

Table 1. Elemental composition of recovered solids after hydrothermal treatments at varied metal cation composition. All the results were collected via ICP-OES.

Sample	C.R.[a]	Si/Al	Na/Al	K/Al	Ca/Al	Cat./Al[b]
PHI-TOB-373-0[c]	0.00	3.13	0.24	0.60	-	0.84
PHI-TOB-373-0[d]	0.00	2.33	0.24	0.34	-	0.58
PHI-TOB-373-0.25	0.25	-	5.27	2.35	0.06	7.68
PHI-TOB-373-0.50	0.50	-	2.73	1.38	0.03	4.13
PHI-TOB-373-0.75	0.75	-	3.99	1.51	0.89	6.40
PHI-TOB-373-1.00	1.00	-	0.45	0.08	0.16	0.69
PHI-TOB-393-0.00	0.00	2.78	0.36	0.64	-	1.01
PHI-TOB-393-0.30	0.30	-	9.07	6.52	0.16	15.75
PHI-TOB-393-0.50	0.50	-	9.38	6.79	0.04	16.21
PHI-TOB-393-0.80	0.80	-	14.19	9.17	4.83	28.19
PHI-TOB-393-1.00	1.00	-	-	-	-	-

[a] Fraction of calcium compared to the total metal cations in the synthesis gel (i.e., $(2 \times Ca^{2+})/(K^{+} + Na^{+} + (2 \times Ca^{2+}))$).
[b] Metal cation content normalized by the aluminum content ((K + Na + Ca)/(Al)).
[c] Synthesis performed at a lower water content to lower the silicon concentration to 0.2 M (more details in Section S.1, Supporting Information).
[d] Synthesis performed at reported molar ratios[13] with a silicon concentration of 3 M (more details in Section S.1, Supporting Information).

References

(1) García, E. J.; Pérez-Pellitero, J.; Pirngruber, G. D.; Jallut, C.; Palomino, M.; Rey, F.; Valencia, S. Tuning the Adsorption Properties of Zeolites as Adsorbents for CO_2 Separation: Best Compromise between the Working Capacity and Selectivity. *Industrial & Engineering Chemistry Ressearch* **2014**, *53* (23), 9860–9874. https://doi.org/10.1021/ie500207s.

(2) Čejka, Jiři; Corma, Avelino; Zones, Stacey. *Zeolites and Catalysis: Synthesis, Reactions and Applications*; John Wiley & Sons, Ltd, 2010.

(3) Cubillas, P.; Anderson, M. W. Synthesis Mechanism: Crystal Growth and Nucleation. In *Zeolites and Catalysis*; John Wiley & Sons, Ltd, 2010; pp 1–55. https://doi.org/10.1002/9783527630295.ch1.

(4) Smaihi, M.; Barida, O.; Valtchev, V. Investigation of the Crystallization Stages of LTA-Type Zeolite by Complementary Characterization Techniques. *European Journal of Inorganic Chemistry* **2003**, *2003* (24), 4370–4377. https://doi.org/10.1002/ejic.200300154.

(5) Cundy, C. S.; Cox, P. A. The Hydrothermal Synthesis of Zeolites: Precursors, Intermediates and Reaction Mechanism. *Microporous and Mesoporous Materials* **2005**, *82* (1), 1–78. https://doi.org/10.1016/j.micromeso.2005.02.016.

(6) Grand, J.; Awala, H.; Mintova, S. Mechanism of Zeolites Crystal Growth: New Findings and Open Questions. *CrystEngComm* **2016**, *18* (5), 650–664. https://doi.org/10.1039/C5CE02286J.

(7) Bozhilov, K. N.; Le, T. T.; Qin, Z.; Terlier, T.; Palčić, A.; Rimer, J. D.; Valtchev, V. Time-Resolved Dissolution Elucidates the Mechanism of Zeolite MFI Crystallization. *Science Advances* **2021**, *7* (25), 1–10.

(8) Yokoi, T.; Mochizuki, H.; Namba, S.; Kondo, J. N.; Tatsumi, T. Control of the Al Distribution in the Framework of ZSM-5 Zeolite and Its Evaluation by Solid-State NMR Technique and Catalytic Properties. *The Journal of Physical Chemistry C* **2015**, *119* (27), 15303–15315. https://doi.org/10.1021/acs.jpcc.5b03289.

(9) Borel, M.; Dodin, M.; Daou, T. J.; Bats, N.; Patarin, J. Formation Domain of SDA-Free Y Faujasite Small Crystals. *New Journal of Chemistry* **2017**, *41* (22), 13260–13267. https://doi.org/10.1039/C7NJ02200J.

(10) Steinfink, H. The Crystal Structure of the Zeolite, Phillipsite. *Acta Crystallographica* **1962**, *15* (7), 644–651. https://doi.org/10.1107/S0365110X62001802.

(11) Hou, J.; Yuan, J.; Xu, J.; Sun, L. Synthesis and Characterization of K-Phillipsite (K-PHI) Membrane for Potassium Extraction from Seawater. *Microporous and Mesoporous Materials* **2013**, *172*, 217–221. https://doi.org/10.1016/j.micromeso.2013.01.034.

(12) Passaglia, E.; Vezzalini, G.; Carnevali, R. Diagenetic Chabazites and Phillipsites in Italy: Crystal Chemistry and Genesis. *European Journal of Mineralogy* **1990**, *2* (6), 827–840. https://doi.org/10.1127/ejm/2/6/0827.

(13) Cichocki, A.; Grochowski, J.; Lebioda, L. Phillipsite-Type Synthetic Zeolite with High Silica Contents and Accompanying Phases. *Kristall Und Technik-Crystal Research and Technology*, 1979, *14*, 9–18. https://doi.org/10.1002/crat.19790140103.

(14) Mitsuda, T.; Taylor, H. F. W. Influence of Aluminium on the Conversion of Calcium Silicate Hydrate Gels into 11 Å Tobermorite at 90 °C and 120 °C. *Cement and Concrete Research*, 1975, *5*, 203–209. https://doi.org/10.1016/0008-8846(75)90001-0.

(15) Elhemaly, S. A. S.; Mitsuda, T.; Taylor, H. F. W. Synthesis of Normal and Anomalous Tobermorites. *Cement and Concrete Research*, 1977, *7*, 429–438.

(16) Hong, S.-Y.; Glasser, F. P. Phase Relations in the CaO–SiO_2–H_2O System to 200 °C at Saturated Steam Pressure. *Cement and Concrete Research* **2004**, *34* (9), 1529–1534. https://doi.org/10.1016/j.cemconres.2003.08.009.
(17) Shaw, S.; Clark, S. M.; Henderson, C. M. B. Hydrothermal Formation of the Calcium Silicate Hydrates, Tobermorite ($Ca_5Si_6O_{16}(OH)_2 \cdot 4H_2O$) and Xonotlite ($Ca_6Si_6O_{17}(OH)_2$): An in Situ Synchrotron Study. *Chemical Geology* **2000**, *167* (1), 129–140. https://doi.org/10.1016/S0009-2541(99)00205-3.
(18) Gabrovšek, R.; Kurbus, B.; Mueller, D.; Wieker, W. Tobermorite Formation in the System CaO, C_3S-SiO_2-Al_2O_3-NaOH-H_2O under Hydrothermal Conditions. *Cement and Concrete Research* **1993**, *23* (2), 321–328. https://doi.org/10.1016/0008-8846(93)90097-S.
(19) Huang, X. A.; Jiang, D. L.; Tan, S. H. Novel Hydrothermal Synthesis of Tobermorite Fibers Using Ca(II)-EDTA Complex Precursor. *Journal of the European Ceramic Society*, 2003, *23*, 123–126. https://doi.org/10.1016/s0955-2219(02)00066-3.
(20) Oleksiak, M. D.; Ghorbanpour, A.; Conato, M. T.; McGrail, B. P.; Grabow, L. C.; Motkuri, R. K.; Rimer, J. D. Synthesis Strategies for Ultrastable Zeolite GIS Polymorphs as Sorbents for Selective Separations. *Chemistry-A European Journal*, 2016, *22*, 16078–16088. https://doi.org/10.1002/chem.201602653.
(21) García, J. E.; González, M. M.; Notario, J. S. Phenol Adsorption on Natural Phillipsite. *Reactive Polymers* **1993**, *21* (3), 171–176. https://doi.org/10.1016/0923-1137(93)90119-Z.
(22) Notario, J. S.; Garcia, J. E.; Caceres, J. M.; Arteaga, I. J.; Gonzalez, M. M. Characterization of Natural Phillipsite Modified with Orthophosphoric Acid. *Applied Clay Science* **1995**, *10* (3), 209–217. https://doi.org/10.1016/0169-1317(95)00025-Y.
(23) Osacký, M.; Pálková, H.; Hudec, P.; Czímerová, A.; Galusková, D.; Vítková, M. Effect of Alkaline Synthesis Conditions on Mineralogy, Chemistry and Surface Properties of Phillipsite, P and X Zeolitic Materials Prepared from Fine Powdered Perlite by-Product. *Microporous and Mesoporous Materials* **2020**, *294*, 109852. https://doi.org/10.1016/j.micromeso.2019.109852.
(24) Mumpton, F. A.; Ormsby, W. C. Morphology of Zeolites in Sedimentary Rocks by Scanning Electron Microscopy. *Clays and Clay Minerals* **1976**, *24* (1), 1–23. https://doi.org/10.1346/CCMN.1976.0240101.
(25) Diez-Garcia, M.; Gaitero, J. J.; Dolado, J. S.; Aymonier, C. Ultra-Fast Supercritical Hydrothermal Synthesis of Tobermorite under Thermodynamically Metastable Conditions. *Angewandte Chemie-International Edition*, 2017, *56*, 3162–3167. https://doi.org/10.1002/anie.201611858.
(26) Huang, X.; Jiang, D.; Tan, S. Novel Hydrothermal Synthesis Method for Tobermorite Fibers and Investigation on Their Thermal Stability. *Materials Research Bulletin* **2002**, *37* (11), 1885–1892. https://doi.org/10.1016/S0025-5408(02)00854-1.
(27) Galvánková, L.; Másilko, J.; Solný, T.; Štěpánková, E. Tobermorite Synthesis Under Hydrothermal Conditions. *Procedia Engineering* **2016**, *151*, 100–107. https://doi.org/10.1016/j.proeng.2016.07.394.
(28) Oleksiak, M. D.; Rimer, J. D. Synthesis of Zeolites in the Absence of Organic Structure-Directing Agents: Factors Governing Crystal Selection and Polymorphism. *Reviews in Chemical Engineering* **2014**, *30* (1), 1–49. https://doi.org/doi:10.1515/revce-2013-0020.
(29) Lechert, H. The PH Value and Its Importance for the Crystallization of Zeolites. *Microporous and Mesoporous Materials* **1998**, *22* (4), 519–523. https://doi.org/10.1016/S1387-1811(98)80014-0.

(30) Donahoe, R. J.; Liou, J. G. An Experimental Study on the Process of Zeolite Formation. *Geochimica et Cosmochimica Acta* **1985**, *49* (11), 2349–2360. https://doi.org/10.1016/0016-7037(85)90235-2.
(31) Houston, J. R.; Maxwell, R. S.; Carroll, S. A. Transformation of Meta-Stable Calcium Silicate Hydrates to Tobermorite: Reaction Kinetics and Molecular Structure from XRD and NMR Spectroscopy. *Geochemical Transactions* **2009**, *10* (1), 1. https://doi.org/10.1186/1467-4866-10-1.
(32) Di Iorio, J. R.; Gounder, R. Controlling the Isolation and Pairing of Aluminum in Chabazite Zeolites Using Mixtures of Organic and Inorganic Structure-Directing Agents. *Chemistry of Materials*, 2016, *28*, 2236–2247. https://doi.org/10.1021/acs.chemmater.6b00181.
(33) Lowe, B. M.; Nee, J. R. D.; Casci, J. L. Crystallization of "Inorganic" ZSM-5 in the System K_2O-Al_2O_3-SiO_2-H_2O. *Zeolites* **1994**, *14* (8), 610–619. https://doi.org/10.1016/0144-2449(94)90116-3.
(34) Jakkula, V. S.; Williams, C. D.; Hocking, T. J.; Fullen, M. A. High Selectivity and Affinity of Linde Type F towards NH^{4+} on Application as a Soil Amendment for Maize Growth. *Microporous and Mesoporous Materials* **2006**, *88* (1), 101–104. https://doi.org/10.1016/j.micromeso.2005.09.001.
(35) Basaldella, E. I.; Tara, J. C. Synthesis of LSX Zeolite in the NaK System: Influence of the NaK Ratio. *Zeolites* **1995**, *15* (3), 243–246. https://doi.org/10.1016/0144-2449(94)00006-E.
(36) Merlino, S.; Bonaccorsi, E.; Armbruster, T. The Real Structure of Tobermorite 11Å: Normal and Anomalous Forms, OD Character and Polytypic Modifications. *European Journal of Mineralogy* **2001**, *13* (3), 577–590. https://doi.org/10.1127/0935-1221/2001/0013-0577.
(37) Yang, Y.; Xu, L.; Lyu, Y.; Liu, X.; Yan, Z. Controllable Synthesis of SAPO-11/5 Intergrowth Zeolite for Hydroisomerization of n-Hexane. *Microporous and Mesoporous Materials* **2021**, *313*, 110857. https://doi.org/10.1016/j.micromeso.2020.110857.
(38) Choi, M.; Na, K.; Kim, J.; Sakamoto, Y.; Terasaki, O.; Ryoo, R. Stable Single-Unit-Cell Nanosheets of Zeolite MFI as Active and Long-Lived Catalysts. *Nature* **2009**, *461*, 246-U120. https://doi.org/10.1038/nature08288.
(39) Li, X.; Han, H.; Xu, W.; Hwang, S.-J.; Lu, P.; Bhan, A.; Tsapatsis, M. Enhanced Reactivity of Accessible Protons in Sodalite Cages of Faujasite Zeolite. *Angewandte Chemie-International Edition* **2022**, *61* (5), e202111180. https://doi.org/10.1002/anie.202111180.
(40) Pahari, S.; Dorneles de Mello, M.; Shah, M. S.; Josephson, T. R.; Ren, L.; Nguyen, H. G. T.; Van Zee, R. D.; Tsapatsis, M.; Siepmann, J. I. Ethanol and Water Adsorption in Conventional and Hierarchical All-Silica MFI Zeolites. *ACS Physical Chemistry Au* **2022**, *2* (2), 79–88. https://doi.org/10.1021/acsphyschemau.1c00026.
(41) Saulat, H.; Song, W.; Yang, J.; Yan, T.; He, G.; Tsapatsis, M. Fabrication of b-Oriented MFI Membranes from MFI Nanosheet Layers by Ammonium Sulfate Modifier for the Separation of Butane Isomers. *Journal of Membrane Science* **2022**, *658*, 120749. https://doi.org/10.1016/j.memsci.2022.120749.
(42) Navrotsky, A. Energetic Clues to Pathways to Biomineralization: Precursors, Clusters, and Nanoparticles. *Proceedings of the National Academy of Sciences* **2004**, *101* (33), 12096–12101. https://doi.org/10.1073/pnas.0404778101.
(43) Navrotsky, A.; Trofymluk, O.; Levchenko, A. A. Thermochemistry of Microporous and Mesoporous Materials. *Chemical Reviews* **2009**, *109* (9), 3885–3902. https://doi.org/10.1021/cr800495t.

(44) Maldonado, M.; Oleksiak, M. D.; Chinta, S.; Rimer, J. D. Controlling Crystal Polymorphism in Organic-Free Synthesis of Na-Zeolites. *Journal of the American Chemical Society* **2013**, *135* (7), 2641–2652. https://doi.org/10.1021/ja3105939.